On the numerical simulation of buoyant convection

By D. K. LILLY, *General Circulation Research Laboratory, U.S. Weather Bureau, Washington*

(Manuscript received October 21, 1961, revised version March 6, 1962)

ABSTRACT

The two-dimensional turbulent vortex generated by release of buoyant fluid from an instantaneous thermal line source has been simulated by machine numerical solution of a complete set of Eulerian gas equations. The equations included turbulent eddy exchange terms, similar to those used by Smagorinsky, which made possible the generation of computationally stable solutions qualitatively and quantitatively resembling the convective "thermals" studied and described by Scorer and Richards. The results of a number of numerical experiments, performed with varying computational approximations, lead to conclusions as to the importance of various sources of numerical errors and the validity of the eddy exchange formulation. The formulation leads to qualitatively good results with the resolution provided by about 1500 grid points, but it has not yet been possible to exhibit the shape-preserving stage assumed in theoretical treatments and found approximately by laboratory experiments. This is probably due in large part to the neglect of the effects of eddies in the third dimension.

1. Goals and general procedure

In this article we present some results of a theoretical investigation of turbulent thermal convection in a compressible fluid (dry air) by means of direct numerical time-integration of a complete set of dynamic equations. Before discussing in detail the methods and results of this investigation we will briefly discuss the position of this type of study in relation to that of more conventional analytic methods. Due to the sequential and initially uncertain nature of the results of this type of investigation we conveniently call it a numerical experiment. One should always keep in mind, however, that (barring code errors) the results are purely logical consequences of the various theoretical approximations and simplifications initially assumed, difficult though it may be to trace through the effects of a particular assumption.

The application of numerical experimentation to physical theory is generally justifiable only when more concise analytic methods have been unproductive or have reached apparent limits of usefulness, but these conditions seem to prevail in the field of turbulent fluid mechanics. Although it would be possible to formulate and numerically integrate sets of differential equations, initial and boundary values, appropriate to a broad range of fluid dynamics phenomena, there would be little merit in going to this considerable labor for cases where general analytic solutions are available. This occurs under various conditions but most generally when the ratio of viscous and diffusive terms to those connected with inertial, advective, and gravitational forces is large, i.e. when the Reynolds and Rayleigh numbers are small. For thermal convective motions the linear solutions have some qualitative significance even for moderately large Rayleigh numbers, several times the critical value for onset of unstable motion. In addition there are some non-linear steady-state analytic solutions, or asymptotic approaches to solutions, available for this range (MALKUS & VERONIS, 1958; KUO, 1960). Thus it is doubtful whether in that regime a numerical initial-value approach would be justified, except perhaps for specific engineering purposes. When the scale and energy of a system become so large that it may be considered turbulent, however, we enter a region rather poorly explained by previously available theoretical methods. Experimental evidence indicates that motions are never steady, and theory generally deals with statistical moments of the flow. A fundamental method of analysis in this regime is based on assumptions of similarity and self-preservation of some of these averaged flow characteristics, and these assumptions frequently lead to simple and experimentally verifiable partial solutions, e.g. BACHELOR (1956). For each particular phenomenon studied, however, there are several constants or functions to be determined experimentally, and no real unifying theory exists to relate these constants and functions from one experimental geometry to another. It should be possible to demonstrate that numerical integration of a single set of differential equations (not necessarily including the unmodified Navier–Stokes equations) with varying boundary and initial conditions can yield solutions corresponding to various experimental phenomena, such as jets, puffs, wakes, and convective bubble- and plume-like thermals. Such a demonstration cannot by itself provide the desired unifying theory. The detailed statistics of the numerical solutions may, however, aid in its formulation, and in any case these statistics must provide a crucial test of such a theory, as for example, PHILLIPS' numerical experiment (1956) aided in verifying the modern theory of the atmospheric planetary circulation.

A logical plan of attack may be divided into three phases as follows:

(1) develop flexible and computationally well-behaved numerical models for simulation of a large class of fluid motions;

(2) test the detailed behavior of these models by means of experiments comparable with and verifiable by results of significant physical experiments; and

(3) try to extend the results or generalize the models to include conditions not adequately reproducible by experiment. Due to conflicting practical expedients the experiments described in this paper include some mixture of each of these phases, but they are mainly directed toward development and testing of a simple model, which will be described in the following section.

In the model to be described a set of Eulerian partial differential equations was approximated by finite difference equations at points evenly spaced in a square or rectangular net. The Eulerian grid-point representation was chosen principally because of its relatively straightforward program coding and the relatively large fund of knowledge available pertaining to its characteristic behavior. The other most reasonable alternative method of representation, that of expansion into orthogonal functions, was rejected principally due to the difficulty of varying the resolution. The principal difficulty usually encountered in the gridpoint formulation is the development of severe and consistent truncation error, leading eventually to a form of computational instability associated with the non-linear terms. PHILLIPS (1959) has shown that the instability may arise from the non-linear interaction of motion components with wave lengths between 2 and 4 times the grid interval. The interaction components which, in the analytic equations, contribute to components with wave lengths less than twice the grid interval are in the finite difference equations "reflected" back into the 2–4 grid interval scales. In this process the total kinetic energy is spuriously increased. The effect is seemingly strongly dependent on the form of the finite difference representation of the non-linear terms.

The physical experiment with which the results of the computations are to be compared is the instantaneous line source buoyant thermal, recently studied by J. M. Richards, and similar in many respects to the point source thermal described in papers by SCORER (1957, 1958) and WOODWARD (1959). The principal differences between the laboratory experimental set-up and the numerical model are in scale and medium. The physical experiment was carried out with a negatively buoyant salt water "bubble" falling through fresh water in a tank about 2 meters in height, whereas the numerical model simulates warm dry air rising through a volume of cooler air of about 4000 meters depth. These differences are not considered crucial, since the tank experiments were originally designed to simulate and verify the SCORER–LUDLAM (1953) hypothesis of bubble-like thermals of the scale of cumulus clouds. A partial theoretical solution exists for the laboratory case and has been essentially verified by the physical experiment. The details will be described in a later section.

2. History

A number of attempts have been made to simulate convective processes by numerical integration of an Eulerian system of equations. One of the earliest and perhaps still most significant was carried out in the mid-1950's in the Los Alamos Scientific Laboratory at the instigation of J. von Neumann. The computations, carried out on the Maniac I computer, involved the simulated overturning of an unstably stratified two-layer miscible incompressible fluid system. The results, only recently published in a widely available journal (BLAIR *et al.*, 1959), should be of great interest to all investigators using such numerical methods. One of the principal purposes of the experiment was to indicate the possibilities and limitations of following a fluid singularity line without actually applying an internal boundary condition. The problem of non-linear computational instability was here encountered in a rather clear-cut form, involving the tendency of the finite difference equations to steepen gradients in regions where they are already steep and to increase total energy in a closed system. The solution found to this problem was to use non-central space differences, oriented according to the direction of flow, as proposed earlier by COURANT, ISAACSON & REES (1952) and LELEVIER (RICHTMYER, 1957). This effectively provides a selective diffusion coefficient, largest in regions of strong velocities, which then damps out small scale motions, prevents unstable steepening, decreases total energy, and smooths the originally infinite gradient between the fluid layers. Since it is expected that small-scale eddies would mix the fluid layers and degrade potential and kinetic energy, through molecular dissipation, to unavailable heat, the behavior of the system was at least qualitatively reasonable.

J. S. MALKUS & G. WITT (1959) have published results of some numerical experiments in which the early stages of a bubble-like atmospheric thermal were simulated. The experiments could be continued only for a few dozen time steps (equivalent, however, to a few hundred in the present experiments) due to the development of non-linear instability, expressed most obviously by the non-conservation of potential temperature in the bubble and its environment. Addition of diffusion and viscosity terms, including a constant eddy exchange coefficient of presumed reasonable magnitude, did not greatly alter the general evolution nor substantially affect the stability properties.

Several investigators have attempted to simulate the development of convective phenomena of the so-called "meso" scale. Of the published studies KASAHARA's work on hurricanes (1960), SASAKI's on squall lines (1960), and ESTOQUE's (1961) sea breeze computations are probably representative of the methods and results so far available. In the first two of these studies a hydrostatically balanced system of equations was used, which allowed stable and unstable gravitational motions, and some effects of moisture condensation were parametrically represented. In both cases the results were highly dependent on the initial conditions, which are rather difficult to establish for this scale of motion. In addition both exhibited linear instability, which severely restricted the usefulness of the results, as well as the period of time for which they could be obtained. It is perhaps arguable whether the instability should be considered physical or computational, but it consisted of the essentially uncontrolled development of approximately cloud-scale disturbances in gravitationally unstable regions. Control of such instabilities can probably be obtained only by proper simulation of the self-limiting effects of entrainment and mixing of air in and around these cloud-scale cells. Since the presently reported experiments are intended to simulate the detailed mechanics of these cloud-scale motions, it is to be hoped that the methods and results will be of some benefit to those dealing with the larger scale manifestations of convective energy release. Estoque's experiments were based on use of a rather unusual hydrostatic system of differential equations, differenced apparently non-centrally over an inhomogeneous anisotropic x–z grid. The computations were apparently stable and the results appeared to be quite realistic.

Methods of prevention of non-linear computational instability in Eulerian systems may be classified as neutral or damped, in reference to their effects on kinetic energy. In the neutral methods the short wave-length interactions which lead to instability are eliminated, either by a complete elimination of all motion components with wavelengths less than 4 grid intervals

(PHILLIPS, 1959), or more recently by use of an energy conserving grid differencing system (SHUMAN, 1960; ARAKAWA, 1962). The damped methods depend on viscous terms, or their equivalents, to remove short wave components continuously but not completely from the fields of variables. The use of a constant viscosity coefficient is not very effective for this purpose because of its relative insensitivity to wave length. The various uncentered space–time difference schemes similar to that of COURANT, ISAACSON & REES have an equivalent effect to a viscosity proportional to the product of velocity and grid point separation. These methods generally have the advantage of being stable without any adjustment of arbitrary coefficients. In some recent planetary-scale numerical experiments Smagorinsky applied certain non-linear viscous terms similar to those devised by von Neumann and Richtmyer (RICHTMYER, 1950) with good results in maintaining computational stability. In addition, however, Smagorinsky has suggested that these terms may in some respects simulate the effects of small-scale eddy transfers, and in particular that the kinetic energy removed from a system by these terms may be similar in amount and distribution to the energy removed by internal friction through the eddy-cascade process. This approach has been followed in the present study and will be discussed further in the next section.

3. Equations and computational scheme

We write the Eulerian momentum, continuity, and density-weighted potential temperature conservation equations in tensor notation as follows, where we allow the indices to take on the values 1 or 3, x_3 being measured in a direction opposite to the force of gravity:

$$\frac{\partial(\varrho u_i)}{\partial t}+\frac{\partial}{\partial x_j}(\varrho u_i u_j)+\frac{\partial p}{\partial x_i}+g\delta_{i3}\varrho=\frac{\partial \tau_{ij}}{\partial x_j}, \qquad (1)$$

$$\frac{\partial \varrho}{\partial t}+\frac{\partial}{\partial x_j}(\varrho u_j)=0, \qquad (2)$$

$$\frac{\partial(\varrho\theta)}{\partial t}+\frac{\partial(\varrho u_j\theta)}{\partial x_j}=\frac{\partial H_j}{\partial x_j}. \qquad (3)$$

Here ϱ is the density, θ the potential temperature, u_i and x_i the ith velocity and direction component respectively, τ_{ij} the ij'th Reynolds stress component, and H_j the eddy heat flux in the jth direction. The pressure, p, is determined by the equation of state, in the form

$$\frac{p}{p_0}=\left(\frac{R\varrho\theta}{p_0}\right)^{cp/cv}, \qquad (4)$$

where p_0 is an arbitrary reference pressure, here set equal to 1000 mb, and c_p, c_v, and R are the specific heats at constant pressure and volume, assumed constant, and the gas constant. We consider the independent variables to be defined as averages over a grid square of side Δ in the x_1x_3 plane, over an infinite distance in the x_2 direction, and over a time interval Δt, and that their spatial and time derivatives are expressible to first-order accuracy by finite difference approximations from grid-point data. The eddy stresses and heat flux are composed of the usual double velocity and velocity-temperature correlations, respectively.

Now further assume that these eddy terms are proportional to mean gradients by eddy viscosity and diffusion coefficients, constant and isotropic within a space-time grid square, and express these fluxes as follows:

$$\tau_{ij}=\varrho K_M\left(\frac{\partial u_i}{\partial x_j}+\frac{\partial u_j}{\partial x_i}-\frac{2\delta_{ij}}{\delta_{ii}}\frac{\partial u_j}{\partial x_j}\right), \qquad (5)$$

$$H_j=\varrho K_H\frac{\partial \theta}{\partial x_j}, \qquad (6)$$

where $\delta_{ii}=2$ in this case, by the summation convention, and K_M and K_H are the (variable) eddy viscosity and heat diffusion coefficients. These coefficients are to be determined from the explicit flow parameters, and the entire physical content of the formal expressions given above must rest on the method of their determination.

As an aid in the discussion we shall exhibit the energy equations corresponding to (1)–(3). The kinetic energy equation, formed by the combination of (1) multiplied by u_i and (2) by u_i^2 is:

$$\frac{\partial E_K}{\partial t}+\frac{\partial}{\partial x_j}[u_j(E_K+p)]-p\frac{\partial u_j}{\partial x_j}+g\varrho u_3 =\frac{\partial}{\partial x_j}(u_i\tau_{ij})-\varrho K_M \mathrm{Def}^2, \qquad (7)$$

where Def^2 is the square of the deformation tensor, equal in two dimensions to

$$\left[\left(\frac{\partial u_1}{\partial x_1}-\frac{\partial u_3}{\partial x_3}\right)^2+\left(\frac{\partial u_1}{\partial x_3}+\frac{\partial u_3}{\partial x_1}\right)^2\right],$$

and $$E_K=\tfrac{1}{2}\varrho u_i^2.$$

The internal energy equation is formed by multiplication of (3) by $p/\varrho\theta$ and application of (4):

$$\frac{\partial E_I}{\partial t}+\frac{\partial}{\partial x_j}(u_j E_I)+p\frac{\partial u_j}{\partial x_j}=\frac{c_p}{R}\frac{\partial}{\partial x_j}\left(\frac{p}{\theta}H_j\right)-\frac{K_H}{\theta}\frac{\partial\theta}{\partial x_j}\frac{\partial p}{\partial x_j}, \qquad (8)$$

where $$E_I=c_v\varrho T.$$

The equation of potential energy is obtained by multiplication of (2) by x_3 to obtain:

$$\frac{\partial E_P}{\partial t}+\frac{\partial}{\partial x_j}(u_j E_P)-g\varrho u_3=0, \qquad (9)$$

where $$E_P=g\varrho x_3.$$

Addition of (7), (8), and (9) yields the total explicit energy equation as follows, where $E=E_K+E_P+E_I$:

$$\frac{\partial E}{\partial t}+\frac{\partial}{\partial x_j}[u_j(E+p)]-\frac{\partial}{\partial x_j}\left[u_i\tau_{ij}+\frac{c_p}{R}\frac{p}{\theta}H_j\right]=-\{E_K:E_E\}-\{E_I:E_E\}, \qquad (10)$$

where the eddy transformation terms

$$\left.\begin{aligned}\{E_K:E_E\}&=\varrho K_m\,\mathrm{Def}^2\\ \{E_I:E_E\}&=\frac{K_H}{\theta}\frac{\partial\theta}{\partial x_j}\frac{\partial p}{\partial x_j}\end{aligned}\right\} \qquad (11)$$

represent the energy transferred to turbulent energy, E_E, through the agencies of eddy viscosity and diffusion, respectively.

In lieu of an equation governing the rate of change of turbulent energy we assume that the adjustments of the eddies to their environment is instantaneous, so that the sum of the transformation terms (11) is identical to the dissipation rate. If these eddies are limited in size by the grid separation then dimensional analysis requires that the eddy viscosity be determined by a product of a grid-scale velocity and this separation. An appropriate such product, for the case of zero heat flow (θ = constant) is

$$K_M=(k\Delta)^2|\mathrm{Def}| \qquad (12)$$

where k is a constant of order unity.

It is to be remembered that Def^2 is computed from finite differences between grid points and therefore is proportional to the two-point velocity correlation more frequently used in turbulence theory. We may further note that if the grid-separation scale lies in an inertial subrange of the energy spectrum, so that the one-dimensional spectral function $E^*(\varkappa)$ is defined by a power law in the wave number $\varkappa$, then Def^2 is proportional to the kinetic energy contained in scales of motion smaller than the grid, i.e.

$$\Delta^2\,\mathrm{Def}^2\propto\int_{1/\Delta}^{\infty}E^*(\varkappa)\,d\varkappa, \qquad (13)$$

as shown by BATCHELOR (1954, p. 120).

If the above integral is identified with the turbulent energy, E_E, then from (12) we see that K_M is proportional to the product of Δ and $\sqrt{E_E}$. Finally, again assuming zero heat flow, so that the first part of (11) is equal to the dissipation rate, ε, it is easily shown from (11) and (12) that

$$K_M=\frac{\varepsilon}{\varrho}(k\Delta)^{4/3}, \qquad (14)$$

corresponding to the power law suggested by RICHARDSON (1926) from atmospheric data and dimensionally similar to HEISENBERG's (1948) expression for homogeneous isotropic turbulence.

The existence of thermal activity and buoyancy effects add great complexity to the eddy exchange problem. The theory of turbulence in thermally stratified fluids is much less well developed than that of shearing turbulence and the body of observational material yields somewhat conflicting results. It is, in fact, doubtful that a universal equilibrium theory can be established to relate turbulent transfers to mean gradients, regardless of scale and for the entire range of the Richardson number. The assumptions we will make essentially imply such a theory; thus we must apply a considerable amount of empiricism, and cannot expect the resulting expressions to be necessarily valid for all geometrical or physical frameworks. We assume that (14) is universally valid for ε equal to the sum of the terms of (11). Upon substitution of these terms into (14) we obtain a more general expression than (12) for the eddy viscosity coefficient, i.e.

$$K_M = (k\Delta)^2 |\mathrm{Def}| \sqrt{1 - \frac{K_H}{K_M}\mathrm{Ri}}, \tag{15}$$

where
$$\mathrm{Ri} = -\frac{\frac{1}{\varrho\theta}\frac{\partial p}{\partial x_j}\frac{\partial \theta}{\partial x_j}}{\mathrm{Def}^2} \approx \frac{\frac{g}{\theta}\frac{\partial\theta}{\partial x_3}}{\mathrm{Def}^2}, \tag{16}$$

the approximation being valid for small Mach numbers only. The ratio K_H/K_M and perhaps also k are unknown functions of the grid Richardson number, Ri. With such a wide degree of freedom (15) obviously represents little but dimensional analysis.

Both (12) and (15) exhibit an obvious similarity to the well-known one-dimensional mixing length boundary layer formulations where k is analogous to the Karman constant. Heated boundary layer formulae, due to Kazansky & Monin (1956) and Ellison (1957) include a constant multiplier of the K_H/K_M ratio, chosen to fit observations in various lapse rate conditions. Ellison shows that the K_H/K_M ratio consistent with this formulation must have a finite limit as $\mathrm{Ri} \to -\infty$ and suggests that it should be proportional to $(\mathrm{Ri})^{-1}$ for $\mathrm{Ri} \to \infty$. For all our experiments $K_H/K_M = 1$ but in some cases (12) was used in place of (15).

Aside from the more-or-less arbitrary determination of the constants k and K_H/K_M there are a number of critical assumptions made in the preceding derivation, all of which are partially invalid under certain circumstances. Some of these are listed below, together with possible methods of their elimination.

(*a*) Viscosity assumption. The assumption of proportionality between eddy fluxes and mean gradients has many well-known exceptions and limitations but also many successful applications. In our use of this assumption, however, the "mean" or explicit fields upon which turbulence is superimposed are themselves fluctuating in time, in contrast to the more usual steady state fields of classical turbulence theory. It is not known to what extent this procedure is valid.

(*b*) Equilibrium assumption. We assume that turbulence is locally dissipated as fast as it is generated, with negligible advective and diffusive effects, but the turbulent energy is always proportional to the squared grid-scale velocity deformation. This is clearly only possible in the limit of vanishingly small turbulent energy. The assumption may be replaced by the introduction of turbulent intensity as an explicit time-dependent variable with production, advection, dissipation, and diffusion terms in its governing equation. This method has been pursued recently and appears to have promise, but no results are given in the present paper.

(*c*) Two-dimensional assumption. The assumption that the grid separation is proportional to the characteristic scale of turbulence implies that larger eddies in the third dimension are of negligible effect. This would appear to put an unreasonable constraint on the eddy diffusion process and may account partially for the apparent lack of approach of the results to the expected power laws as shown later. The proper remedy to this problem, use of a three-dimensional net, is nearly unavailable for economic reasons. A more empirical approach might consist of the use of a characteristic turbulence scale determined by a dimension of the largest scale disturbances or by the distance from boundaries, or both.

(*d*) Richardson criterion assumption. We assume that if $\mathrm{Ri} > 1$ then K_M and therefore ε vanish. This criterion, or any other of the sort seems to neglect such diffusive and dissipative phenomena as the "breaking" of gravity waves on an inversion. The use of a turbulent intensity equation appears to alleviate this situation partially, but the effect of positive static stability upon turbulent flow and vice versa remains a highly uncertain subject.

The boundary conditions specified for the present series of computations are the so-called "free surface" and "insulated" boundary conditions, i.e.

$$u_i = 0 \quad \text{at} \quad x_i = 0, L_i, \tag{17}$$

$$\tau_{ij} = 0 \quad \text{for} \quad i \neq j \quad \text{at} \quad x_i = 0, L_i, \tag{18}$$

$$\frac{\partial \tau_{ii}}{\partial x_i} = 0 \quad \text{at} \quad x_i = 0, \mathrm{L}_i, \tag{19}$$

$$\frac{\partial p}{\partial x_i} + g\delta_{i3}\varrho = 0 \quad \text{at} \quad x_i = 0,\ L_i, \tag{20}$$

$$H_i = 0 \quad \text{at} \quad x_i = 0,\ L_i. \tag{21}$$

These conditions presume reflective symmetry across the lateral boundaries, so that a disturbance centered at or near a boundary acts as if it were accompanied by its mirror image across the boundary. This property can be, and is, taken advantage of to reduce the computational requirements by half for idealized disturbances with no basic horizontal flow or mean lateral temperature gradients.

The method of numerical formulation of a set of equations similar to (1)–(6) has been outlined in a previous paper (LILLY, 1961). A space-time staggered grid network is set up such that, if the grid points are considered as centers of squares on a checkerboard, all dependent variables are defined at a given time on the black squares, and for one time interval later (or earlier) on the red squares. Using this system a time and space central differencing scheme can be applied to the differential equations written in the flux divergence form, as (1)–(3), with spatial or time interpolations necessary in the density term of the vertical motion equation. The advantage of this system over a non-staggered grid is in the reduction of 50 per cent of the computation required for a given resolution. Qualitative and quantitative comparisons of this system, the non-staggered grid system, and another staggered grid system proposed by ELIASSEN (1956) were made in the referenced paper. Linear computational stability criteria are essentially identical for most systems based on (1)–(4), and require essentially that

$$\Delta t < \frac{\Delta}{\sqrt{2}\,c_s}, \tag{22}$$

where c_s is the speed of sound and Δt is the time interval (one-half of a central differenced time step). Non-linear computational instability will ensue in the absence of viscosity-diffusion terms but it is well controlled by the use of (5)–(6) and (12) or (15) in addition to the physical function of these terms. A property of the differential equations is that volume integrals of the dependent variables depend only on boundary conditions. The same property is true of sums of the finite difference equations defined at grid points, provided that they are expressed in the flux-divergence form and that certain extra computational boundary conditions are imposed. These conditions, discussed by SMAGORINSKY (1958), impose no physical constraint upon the internal points, and generally only involve the use of one-sided difference approximations to derivatives across boundaries. These conditions have been applied to the numerical formulation, and as a result total mass and total heat are conserved exactly except for round-off error. This property is used as a check for machine and programming errors and also assures the accuracy of heat flux computations.

4. Theoretical and laboratory results

The theory of turbulent buoyant thermals has been investigated largely by means of similarity and dimensional analysis principles. In general this method describes at best the gross character of the motions and leaves certain non-dimensional coefficients and functions to be determined by experiment. A convenient table of some of the more significant results is given by SCORER (1959). For the instantaneous line source thermal in an incompressible fluid the following proportionalities are obtained.

$$\left.\begin{aligned} & x \propto z \propto \iint E_K\,dx\,dz \propto \iint E_P\,dx\,dz \propto t^{1/3}, \\ & \mathrm{Re} \propto \sqrt{\mathrm{Ra}} \propto t^{1/3}, \\ & \mathrm{Ri} = \text{constant}, \\ & w \propto \iint \frac{\partial E_K}{\partial t}dx\,dz \propto \iint -\varepsilon\,dx\,dz \propto t^{-1/3}, \\ & \frac{dw}{dt} \propto \Delta\varrho \propto t^{-4/3}, \end{aligned}\right\} \tag{23}$$

where x and z may represent horizontal and vertical displacements, from a vertical origin, of any definable feature, w may correspond to any velocity measurement, $\Delta\varrho$ may represent any measure of local or average buoyancy, Re, Ra, and Ri are characteristic Reynolds, Rayleigh, and Richardson numbers, E_K and E_P are the kinetic and potential energies, and ε is the rate of dissipation to internal energy. From experimental measurements SCORER

TABLE 1. *Experimental parameters and conditions.*

Expt. no.	Resolution	Initial disturbance height, m	Frictional terms: Type	K or k	Ri Coeff.	Density inter-polation	Time extent, min	Computational stability
3	Low	1000	None	—	—	2-point	0–16	Unstable after 8 min
7	Low	1000	Laminar	$K = 250\,m^2/sec$	—	2-point	0–16	Stable
8	Low	1000	Laminar	$K = 50\,m^2/sec$	—	2-point	0–16	Unstable after 12 min
10	Low	1000	Turbulent	$k = 0.5$	1	2-point	0–40	Stable
13	Low	1000	Turbulent	$k = 0.25$	1	2-point	0–16	Unstable (?)
14	Low	1000	Turbulent	$k = 1.0$	1	2-point	0–16	Stable—strong damping
15	Low	—	None	—	—	2-point	20–36	Unstable
16	Low	—	Turbulent	$k = 1.0$	1	2-point	20–36	Stable
17	Low	—	Turbulent	$k = 0.25$	1	2-point	20–34	Unstable?
21	Low	1000	Turbulent	$k = 0.5$	1	4-point	0–20	Stable
23	Low	1000	Turbulent	$k = 0.5$	1	Time	0–32	Stable
24	Low	1000	Turbulent	$k = 0.5$	0	Time	0–20	Slightly unstable
28	Low	—	Turbulent	$k = 0.5$	0	Time	20–34	Stable
100	High	500	Turbulent	$k = 0.5$	1	4-point	0–20	Stable
101	High	1000	Turbulent	$k = 0.5$	1	4-point	0–20	Stable

(1959) quoted rough numerical coefficients relating some of these features, as follows:

$$\left.\begin{aligned} z_c &= 2.25\,r, \\ w_c &= 0.8\sqrt{g\bar{B}r}, \\ \bar{B} &= \iint \Delta\varrho\, dx\, dz / 2.5\bar{\varrho} r^2, \end{aligned}\right\} \tag{24}$$

where z_c and w_c are the initial height and velocity, respectively, of the thermal cap or front, r is the thermal's maximum horizontal extent, and $\bar{B}$ and $\bar{\varrho}$ are the mean fractional buoyancy and mean density, respectively. Later work (RICHARDS 1962) has shown that the coefficients may vary considerably between, but not within, experiments. A comparison between some of Richards' results and our computed results is given in Table 2.

We may note that even though the thermal is decelerating, it is expanding so rapidly that its kinetic energy is increasing at almost half the rate of decrease of potential energy. The remainder of the released potential energy is being continuously degraded through turbulence and viscosity into unavailable internal energy. This energy dissipation–production ratio of one-half to two-thirds may also be inferred from the results of buoyant plume experiments. It is a feature which should be fairly accurately reproducible by a suitable numerical model.

Before attempting to compare the laboratory and the numerical results we should note several differences in experimental conditions which will cause unavoidable discrepancies. First, the physical experiment is always performed with less than ideal initial conditions, that is the fluid in the thermal and in the tank will have initial velocity fields and density gradients. These irregularities are maintained or selectively amplified in some cases, so that no two realizations of the experiment are identical. The numerical calculation, on the other hand, is started with a completely symmetric idealized disturbance in motionless, exactly zero lapse conditions, except for round-off errors in the 8th decimal place. Further, the numerical system probably cannot react to small scale irregularities in a physically realistic manner because the eddy stress terms are themselves based on integral averages of infinitely many realizations. The truncation error of the numerical calculations in the "low" resolution experiments to be discussed is such as to account reasonably well for disturbance components with half-wavelengths of no less than ¼ of the experiment depth. Thus the numerical results might be expected to show much less detail than any individual physical realization.

A less significant cause of discrepancy, which should not, however, be completely ignored, is associated with the effects of molecular viscosity and diffusion on the laboratory thermal. If the initial density disturbance has a relative buoyancy of about 5 per cent and an initial radius of the order of 2 cm, the initial

Reynolds number, defined as $w_c r/\nu$, will be about 1600. Relations (23) show that $\mathrm{Re} \propto r^{1/2}$, so that if the final radius equals 50 cm, then $\mathrm{Re} = 8000$. These values are undoubtedly in the turbulent regime, but for scales of less than 10 per cent of the radius of the thermal laminar effects should be evident. In the three dimensional axially symmetric thermal, for which the dimensional relationships indicate a constant Reynold's number, the writer is convinced from personal observation that laminar effects are significant in some details of the flow patterns.

The most noticeable qualitative difference between the physical and numerically simulated results, however, is found in the behavior of the thermal's top and side boundaries. This involves both the initial conditions and the laminar effects discussed above, and in addition the method of parametric simulation of turbulent transfer. The laboratory thermal invariably maintains a sharp and well-defined, though irregular, front and side boundary, and one somewhat less well defined to the rear. The density within this boundary exhibits relatively small variations, certainly within the same order of magnitude as the mean. Actually the visible boundary is also the boundary layer of the turbulent region, and motion outside is nearly potential flow, as in the case of turbulent jets and other developing boundary layer flows. The width of such boundary layers according to CORRSIN & KISTLER (1955) is of the order of Kolmogoroff's smallest scale and is just detectable in the laboratory experiment, although it would be negligibly small for the free atmosphere cloud scale. The numerical analogue, however, exhibits no well-defined thermal or turbulence boundary and the density varies continuously throughout a substantial portion of the available space. It is doubtful whether the existence of this boundary layer can be *satisfactorily* simulated by Eulerian numerical models, but it also seems unreasonable to expect this neglect to seriously disturb the energetics of the simulated motions. A somewhat comparable problem to this is that of the representation of frontal discontinuities in planetary general circulation experiments and numerical forecasting.

5. Results of computations

Since the purpose of this series of experiments was to compare the performance of several slightly different formulations with each other and with the laboratory results, the basic physical parameters and boundary and initial conditions were left essentially unchanged throughout the series. These conditions were designed to partially simulate the behavior of Richards' two-dimensional thermals, and also to essentially duplicate the conditions assumed in Malkus and Witt's experiment. Due to the use of a system of gas equations allowing sound propagation, in order to avoid excessively small time steps it was practically necessary to deal with a much larger scale of motion than occurred in either of the similar experiments mentioned above. For what we will call the low-resolution experiments two dimensional motions were confined to a slab 3750 meters high by 7500 meters wide divided into grid squares 250 meters on a side. One second time steps were used. The high-resolution experiments reported here were conducted in a slab 3875 meters high by 11,750 meters wide divided into 125 meter grid squares, and the time steps were one-half second. The boundaries were assumed to be solid, frictionless, and insulated, according to (17)–(21). The system was assumed to be initially motionless and the pressure field was prescribed in hydrostatic equilibrium with a constant potential temperature of 290°K, which was the assumed initial potential temperature everywhere except in the disturbance region. The disturbance, applied on the density and potential temperature fields with $\varrho\theta$ undisturbed, was proportional to the cosine squared in both directions, from the maximum to the *first* zero, and was centered along the symmetry line on the lower boundary. In all experiments except no. 100 this disturbance was confined to an area 1000 meters high and 1000 meters on either side of the center line, with a maximum amplitude in the density field of $5 \cdot 10^{-6}$ g/cm^3, corresponding to approximately 1.2°C in the potential temperature field. In experiment no. 100 the same total mass deficit was used but the disturbance was confined to an area one-fourth as large, so that the maximum potential temperature amplitude was about 4.8°C.

Table 1 summarizes other properties of the various experiments to be discussed. The first nine experiments listed and nos. 24 and 28 were performed in order to establish the effects of various methods of simulating viscosity and

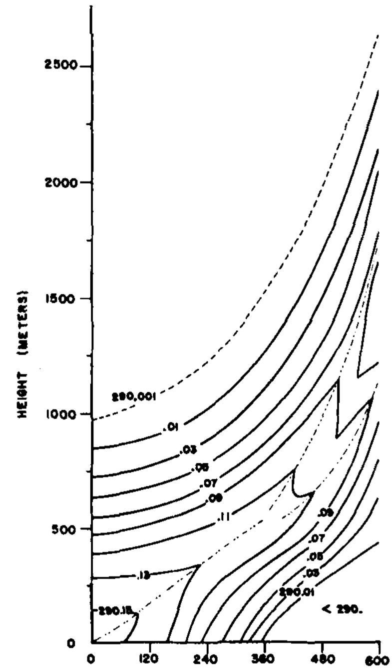

FIG. 1. Experiment 3. Horizontally averaged potential temperature as a function of height and time.

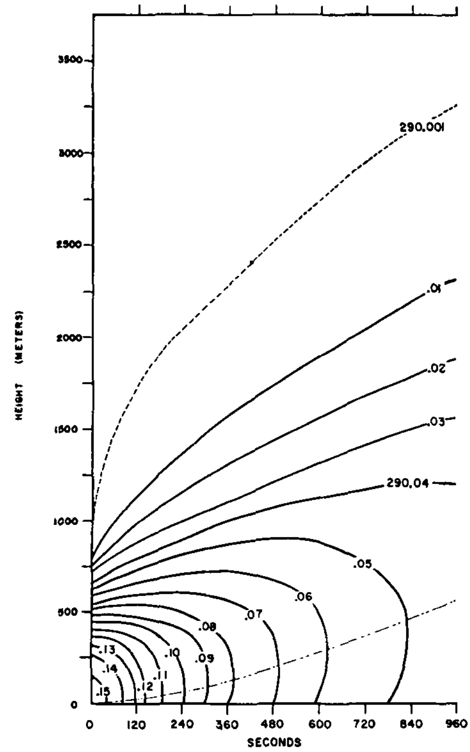

FIG. 2. Experiment 7. Horizontally averaged potential temperature as a function of height and time.

diffusion. Experiments nos. 21 and 23 tested the sensitivity of the system to various methods of interpolation of the density term in the vertical motion equation. In the last two experiments higher spatial resolution was used in an attempt to minimize truncation errors and indicate the approach to an analytic solution. We will now describe some of the details of these computational results.

Experiment 3 was performed with no viscous or diffusive terms. As expected, and as found by Malkus and Witt, truncation errors in the non-linear terms rapidly and severely affected the results, which lost all physical significance after 8–10 minutes when the total energy began to increase. Experiments nos. 7 and 8 included viscous terms but the viscosity-diffusion coefficient was a specified constant instead of being computed by equation (7). The smaller of the two coefficients tried, 50 m^2/sec, was insufficient to maintain computational stability. The larger coefficient, 250 m^2/sec, maintained computational stability but at the cost of most of the non-linear effects of the physical system.

Figs. 1 and 2 are time sections of the horizontally averaged potential temperature for experiments nos. 3 and 7, respectively. In the frictionless case the general shape of the isolines is parabolic, indicating non-dissipative acceleration. At the same time the severe effects of truncation errors are evident in the tendency toward splitting of the maximum and values below 290° near the bottom after 6 minutes. After 10 minutes the patterns became hopelessly complex as computational instability developed. Experiment no. 7, on the other hand, follows an entirely different pattern of development, corresponding more nearly to that of Fickian diffusion superimposed upon a very slowly accelerating ascent. The characteristic Rayleigh number, based on the height and temperature differences between the maximum potential temperature and the 0.005 degree disturbance isoline directly above it, increases from an initial value of 600 to 1800. These

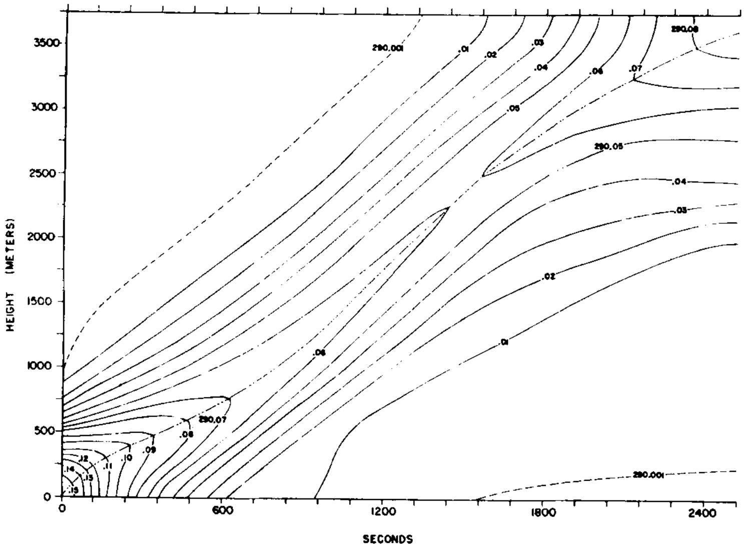

FIG. 3. Experiment 10. Horizontally averaged potential temperature as a function of height and time.

values are in the critical range where heat is transferred about as effectively by diffusion as by convection. The computed solution has very little resemblance to convective motions observed in a real turbulent fluid.

Computations show that in the stable case, experiment no. 7, the *grid* Reynolds number remained everywhere less than unity, while in no. 8, which became computationally unstable, it exceeded this value considerably in some areas. It may also be noted that (12) defines K_M in such a way that the grid Reynolds number is *everywhere* of order unity. The difference in results, then, must be due to the much larger damping by a constant viscosity coefficient in regions of smaller gradients.

In experiments nos. 10, 13, and 14 the eddy viscosity and diffusion form was used, as

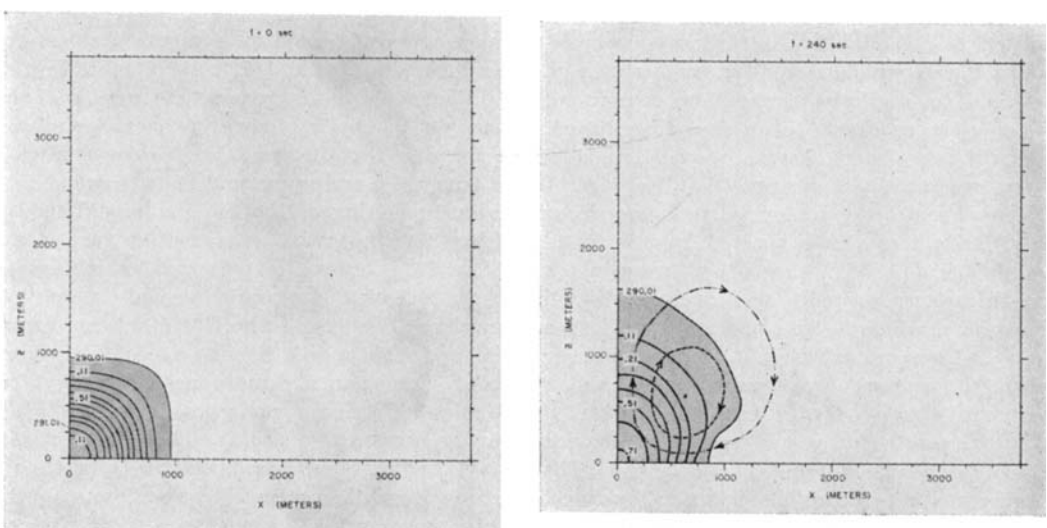

a 0 min b 4 min

FIG. 4*a–f*. Experiment 10. Maps of the momentum stream and potential temperature fields at 4–8 described by equation (15) with K_H/K_M arbitrarily set equal to unity, and with k varied over a factor of 4. There seemed at this time to be no purely objective method of deciding an optimum value for k, but a subjective evaluation of the experimental results favored the intermediate value. The low value did not seem to preserve computational stability properly; the potential temperature maximum, as it rose, tended to split vertically and the upper maximum then intensified, while below the lower maximum appeared a spurious minimum of substantially less than the lowest initial value. These effects were quite similar to those obtained without friction though less intense. When k was made equal to unity, on the other hand, computational stability was very well preserved, but motions appeared to be too severely smoothed. The results for $k = 0.5$ were therefore considered most promising, and computations of experiment no. 10 were continued through the development, ascent, and beginning decay stages of the thermal element. Maps of the approximate streamlines and potential tem-

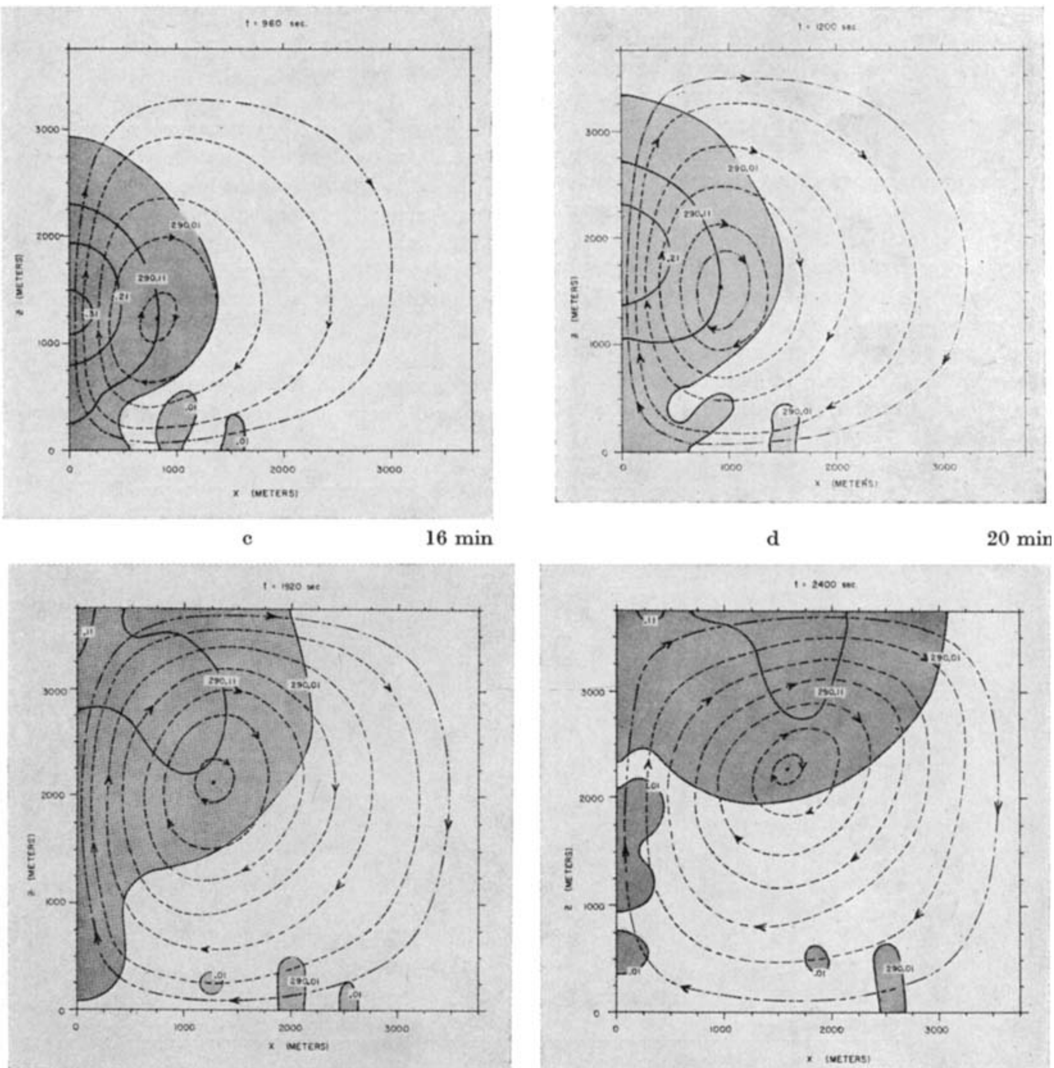

c 16 min

d 20 min

e 32 min

f 60 min

minute intervals. Stream lines are drawn at intervals of 2000 g/cm sec.

perature field at 4–8 minute intervals are presented in Fig. 4*a–f*. Each map displays only the right half of the net, the left half being an exact mirror image. Description of the detailed results of this experiment will be made later, in comparison with the high resolution experiments. The system remained computationally stable, and noticeable effects of truncation error were mainly restricted to the small positive temperature deviation areas (and some similar negative ones), appearing near the bottom of all the maps after 8 minutes. These generally consist of one or two grid points each, with amplitudes of 0.02 degrees or less.

Fig. 3 is a time section of the horizontally averaged potential temperature for experiment no. 10. We observe that the thermal maximum accelerates initially, then rises at a nearly constant rate and decelerates near the top. The maximum temperature deviation decreases rapidly at first, then more slowly, and increases toward the end as the warm air spreads out along the upper boundary. If the disturbance were in shape-preserving equilibrium relations (23) indicate that the height of the temperature maximum would be proportional to $t^{2/3}$, and its value to $t^{-2/3}$ (from multiplication of x and $\Delta\varrho$). These relations, if attained at all, are only momentarily so, and evidently the grid resolution is insufficient to describe the equilibrium state, but the model obviously comes much closer to this state than possible in either the frictionless or linear frictional models. Another aspect of the results is illustrated by Fig. 5, which is a time section of the horizontally averaged heat flux contributions due to the explicit motion terms and the eddy exchange terms. The explicit or disturbance flux, $\iint \varrho u_3 \;\theta\, dx_1 dx_3 / \iint \varrho\, dx_1 dx_3$, is shown by the heavy lines and the eddy flux, $\iint \varrho K_H(\partial\theta/\partial x_3)\, dx_1 dx_3 / \iint \varrho\, dx_1 dx_3$, by the light lines. The latter is obviously much smaller than the former most of the time but the reverse is true in the early stages, where motion amplitudes are negligible and temperature gradients are large. It may also be noted that the maximum of the eddy flux is located above the maximum disturbance flux, that is near the cap or front of the thermal. This corresponds well with SCORER's (1957) observations that maximum turbulent mixing and entrainment of outside fluid occur in this region.

As we have seen the first few minutes of the experiments with $K_H/K_M = 1$ are dominated by strong diffusive heat transfer and rapid expan-

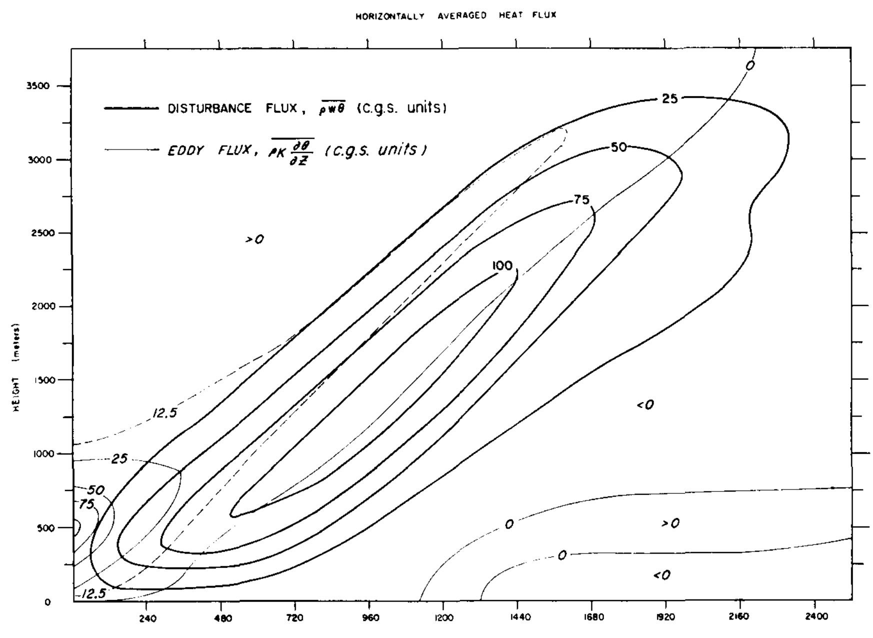

FIG. 5. Experiment 10. Horizontally averaged disturbance and eddy diffusive heat flux as a function of height and time. Units are g deg/cm².

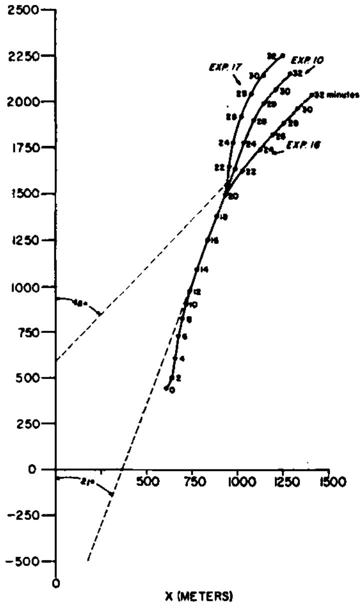

FIG. 6. Trajectories of the vortex centers for experiments 10, 16, and 17. Tangents are drawn to the straight line portions of the 10 and 16 trajectories.

sion and dilution of the thermal element without much motion. Due to the highly dubious correctness of the equilibrium assumption and the K_H/K_M ratio, these early events probably lack much physical significance. In order to further test the effects of variable k, experiments nos. 15, 16, and 17 were performed. For these the equations were identical to those used in nos. 3, 14, and 13, respectively, but the input data

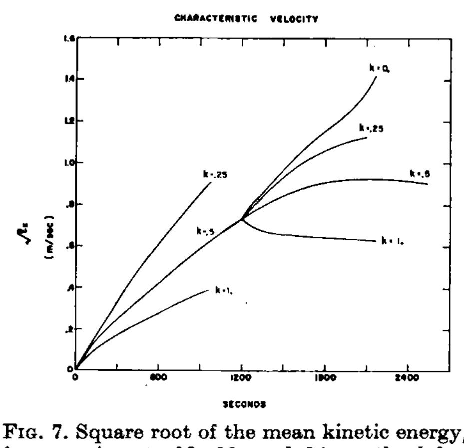

FIG. 7. Square root of the mean kinetic energy/mass for experiments 13, 10, and 14 on the left (from above) and 15, 17, 10, and 16 on the right (from above).

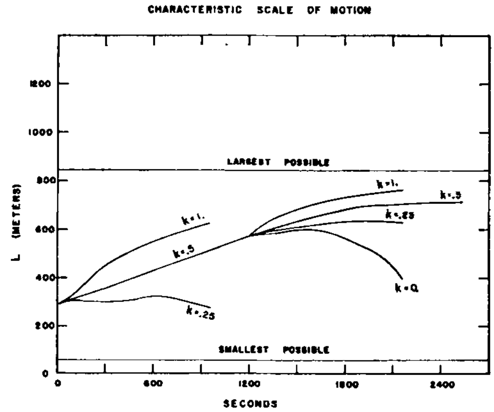

FIG. 8. Square root of the ratio of mean kinetic energy to mean square deformation for experiments 13, 10, 14 on the left (from below) and 15, 17, 10, and 16 on the right (from below). The largest and smallest possible values are constrained by the size of the experimental net and the grid square, respectively.

was taken from the results of no. 10 ($k = 0.5$) at $t = 20$ minutes, when motions were relatively well developed and the element occupied a large part of the area. The results were qualitatively about as expected, though the quantitative differences were surprisingly large. Comparative trajectories of the vortex centers in experiments nos. 10, 16, and 17, shown in Fig. 6, illustrate the immediate effects of the eddy exchange terms on the explicit dynamics. Fig. 7 shows time graphs of the square root of the mean kinetic energy per unit mass for experiments nos. 10, 13, 14, 15, 16, and 17, while Fig. 8 shows the corresponding values of a characteristic length scale of the motions, that is the square root of the ratio of mean kinetic energy to mean square deformation or mean square vorticity (in the absence of significant sonic energy the two are almost identical). From these it is evident that variation of k exerts a strong immediate influence on the energy dissipation and on the energy amplitude itself.

It was presumed that, given sufficient resolution, the large scale energetics must eventually become independent of the size, and probably the form, of the dissipation terms, provided the latter assure computational stability. Therefore the tentative conclusion was that we had not allowed for sufficient separation between the scale of motions containing significant energy and that which most effectively trans-

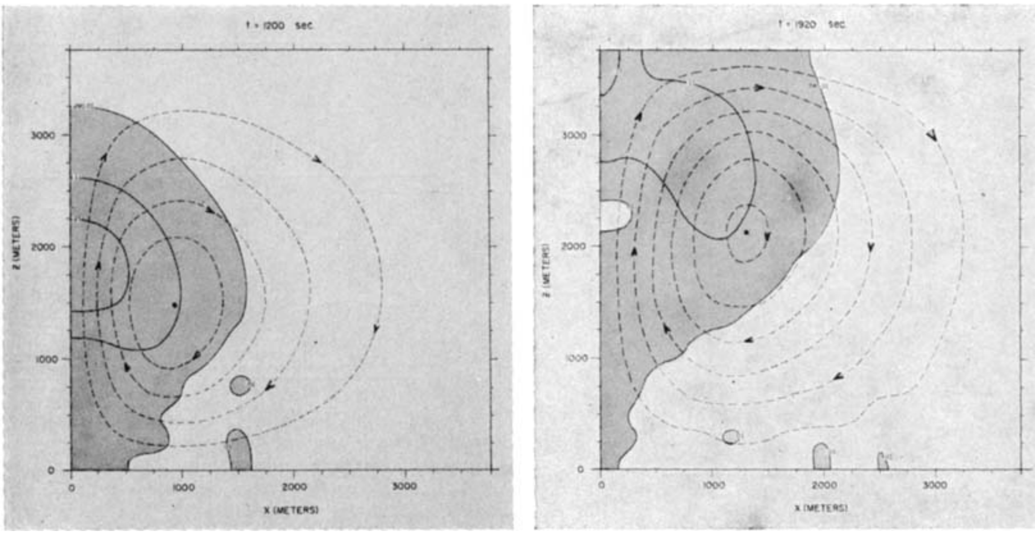

a b

FIG. 9*a*, *b*. Experiment 23. Maps 20 and 32 minutes, respectively. The fields and scaling are as in Fig. 4.

fers energy out of the system. The latter is centered around wavelengths of 4 Δ in the difference scheme used. The largest wave lengths of the system are in this case 30 Δ, giving a separation factor of, at most, 7.5. In the high resolution experiments this factor is doubled.

Experiments nos. 21 and 23 tested the effects of using different interpolation formulae for the linear density term in the vertical equation of motion. In no. 10 a vertical two-point formula had been used, so that if subscripts l and m represent the column and row of the grid location, respectively, and superscript (n) the time index, we would replace $\varrho_{l,m}^{(n)}$ in the finite difference approximation to (1) by $\frac{1}{2}(\varrho_{l,m+1}^{(n)} + \varrho_{l,m-1}^{(n)})$. For no. 21 it would be replaced by $\frac{1}{4}(\varrho_{l+1,m}^{(n)} + \varrho_{l-1,m}^{(n)} + \varrho_{l,m+1}^{(n)} + \varrho_{l,m-1}^{(n)})$ and for no. 23 by $\frac{1}{2}(\varrho_{l,m}^{(n+1)} + \varrho_{l,m}^{(n-1)})$. All other terms were calculated in the same manner as in no. 10. As might be anticipated, differences were most noticeable in the early stages when the disturbance was effectively linear and confined to just a few grid points. In the spatial interpolation cases the initial acceleration field was slightly diffused by the interpolation. The differences between the forms became negligible later. After 20 minutes the mean kinetic energy, mean square vorticity, maximum potential temperature deviation, and nearly all other significant features were identical to within one or two per cent. Figs. 9*a*, *b* are streamline-isentrope maps of experiment no. 23 at 20 and 32 minutes, corresponding respectively to figures 4*d*, *e* for experiment no. 10. It appears that we may consider the results of other experiments in this series to be independent of the method of interpolation of this linear term.

Experiments nos. 24 and 28 were performed to test the influence of the Richardson number terms in the eddy exchange coefficients. In all previous experiments (15) had been used with the K_H/K_M ratio arbitrarily set equal to unity. In this formulation all dissipation vanished for $\mathrm{Ri} \geq 1$. An apparent slight tendency toward instability appeared in the region of large positive Ri under the thermal maximum, suggesting that damping should be increased in this region. This is also indicated by Ellison's conclusions for large positive Ri. Before considering possible functional forms of dependence of K_H/K_M on Ri we tested the effects of complete elimination of the stratification terms in the mixing coefficients. Thus experiment no. 24 was performed with K_M and K_H both obtained from (12), and with initial data and other features the same as in no. 23 (thus essentially similar to no. 10). As expected, the early stages of development were much less subject to diffusion effects in this case, since the exchange coefficients were initially zero. Comparison of figures 9*a* and 10, depicting the streamlines and isen-

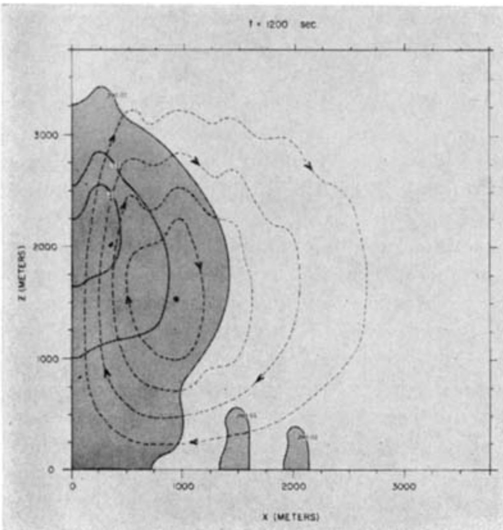

FIG. 10. Experiment 24. Map at 20 minutes.

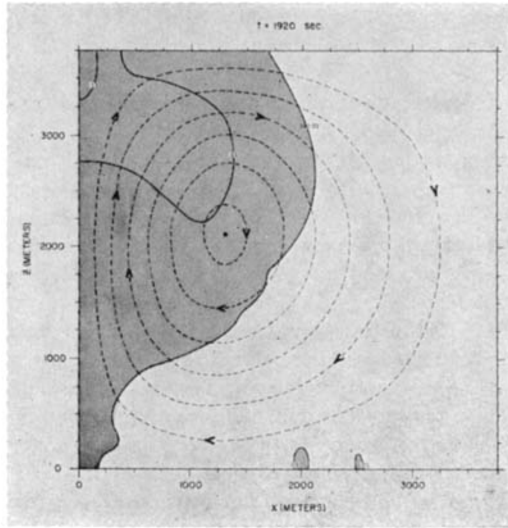

FIG. 11. Experiment 28. Map at 32 minutes.

tropes of nos. 23 and 24 at 20 minutes, indicate that the pure deformation mixing coefficient was insufficient to completely damp computational instabilities in the thermally unstable part of the field. On the other hand the irregularities in the thermally stable area were essentially eliminated in no. 24. For experiment no. 28 input data was taken from the results of no. 23 at 20 minutes, and the pure deformation mixing was again applied. In this case the results differed little from those of no. 23 in important details or integral properties. Figs. 9*b* and 11, comparative maps of nos. 23 and 28 at 32 minutes, show that in the latter some smoothing has again occurred underneath the thermal, but the appearance of the upper part is virtually identical in the two. It is therefore suggested that, except in the initial stages and in stably stratified regions, the effects of the Richardson coefficient terms are relatively small. This suggestion is further confirmed by a comparison of values of the ratio of the transformations of kinetic and potential to eddy energy. This ratio may be considered to define the negative of the averaged grid-scale flux Richardson number, $\widetilde{Rf}$, i.e.

$$\frac{\iint \{E_P : E_E\}\,dx_1\,dx_3}{\iint \{E_K : E_E\}\,dx_1\,dx_3} = \frac{\iint \frac{K_H}{\theta}\frac{\partial p}{\partial x_j}\frac{\partial \theta}{\partial x_j}}{\iint \varrho K_M \,\mathrm{Def}^2\,dx_1\,dx_3}$$

$$= -\frac{\tilde{K}_H}{\tilde{K}_M}\,\mathrm{Ri} = -\widetilde{\mathrm{Rf}} \qquad (25)$$

Fig. 12 illustrates this ratio as a function of time for experiments nos. 23 and 28 and shows that it falls below 0.2 after the initial acceleration period. Thus the neutral stability formula-

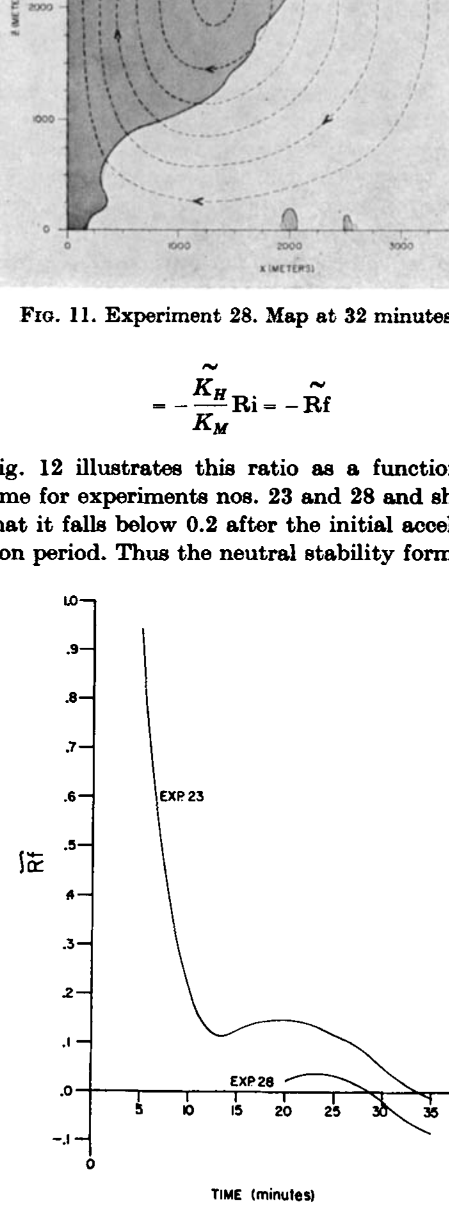

FIG. 12. Ratios of the mean heat and momentum dissipation, experiments 23 and 28.

tion may serve our needs adequately throughout most of the disturbance region.

The remainder of this section will be devoted to detailed description and comparison of experiments nos. 10, 100, and 101 with each other and with appropriate theoretical and laboratory results. Figs. 4, 13, and 14 illustrate the development of the stream and thermal fields for these experiments. This development may be divided into four fairly distinct stages as follows:

(1) Signal propagation. In a compressible medium the maximum signal propagation speed is that of sound, so that no motion is observed at a point until the initial sound wave passes. The sound wave itself has negligible energy when the disturbance is set into the ϱ-field. After about 15 seconds it has traversed the entire area and the initial stream acceleration field has been established.

(2) Acceleration. Initially the motions are linearly accelerating and spreading out by essentially constant exchange coefficients. After a few minutes the thermal maximum separates from the bottom and accelerates upward. The end of this stage is characterized by the splitting in two of the potential temperature maximum and formation of the typical "mushroom" shape.

The experiments performed by Malkus and Witt concerned thermals in this stage of development.

(3) Approach to similarity and shape preservation. The various relationships predicted by similarity theory are not approached uniformly, nor attained simultaneously. Apparently the first to appear is a uniform and constant angle of expansion, most conveniently shown by a trajectory map of the vortex center. Fig. 15 shows these trajectories for experiments nos. 10, 100, and 101 respectively. Other features, especially those involving derivatives and products of quantities, may not exhibit the predicted similarity behavior until considerably later or in some cases not at all in the numerical experiments so far performed.

(4) Spreading out and dissipation. This stage commences when the upper boundary begins to noticeably affect the motions below. Apparently this happens when the center of the thermal is about one diameter removed from the boundary. The final dissipation occurs after the warm air has spread out along the boundary and begins to oscillate as a damped gravity wave. The beginnings of this stage are seen in the last few minutes of no. 10.

Initial qualitative and quantitative evaluations of the results of experiment no. 10 indicated that the resolution was insufficient to adequately describe the similarity stage and approach thereto. If the streamline-isentrope maps are closely examined one may suspect that the acceleration and spreading-out stages described above are immediately successive, if not overlapping. Quantitative evaluations, based on material to be discussed in this section, confirm this suspicion and show that the similarity stage is approximated by few, if any, of the significant parameters. Further, it is unlikely that much improvement in this respect could be obtained by altering the initial disturbance, since this would be countered by the intense diffusive expansion in the first few minutes. Experiments nos. 100 and 101 were performed, therefore, as an attempt to evaluate and partially alleviate the resolution inadequacy. In no. 100 the number of disturbance grid points remained the same as in no. 10, so that the disturbance had effectively twice as much room in which to travel and expand before reaching the top. In no. 101, on the other hand, the same physical disturbance dimensions were used as in no. 10, but with doubled resolution it was hoped that the initial development would be less strongly effected by the parametric eddy diffusion and its associated physical and numerical approximations. Additionally, the lateral extent of the computation net was increased by 50 per cent for both experiments, in an attempt to eliminate lateral boundary considerations. Results indicate that this attempt was successful, as the tangential velocities near the lateral boundaries are generally two orders of magnitude less than the maxima.

Perhaps the first apparent conclusion that may be drawn from comparisons of the maps is that the results of experiments nos. 100 and 101 bear greater similarity to each other than either does to no. 10. Even though the initial disturbance conditions of nos. 10 and 101 are identical except for truncation error, the increased resolution of the latter evidently overrides all other factors. We will substantiate this conclusion further by examination of Figs. 16*a*, *b*, *c*. These are time sections of the

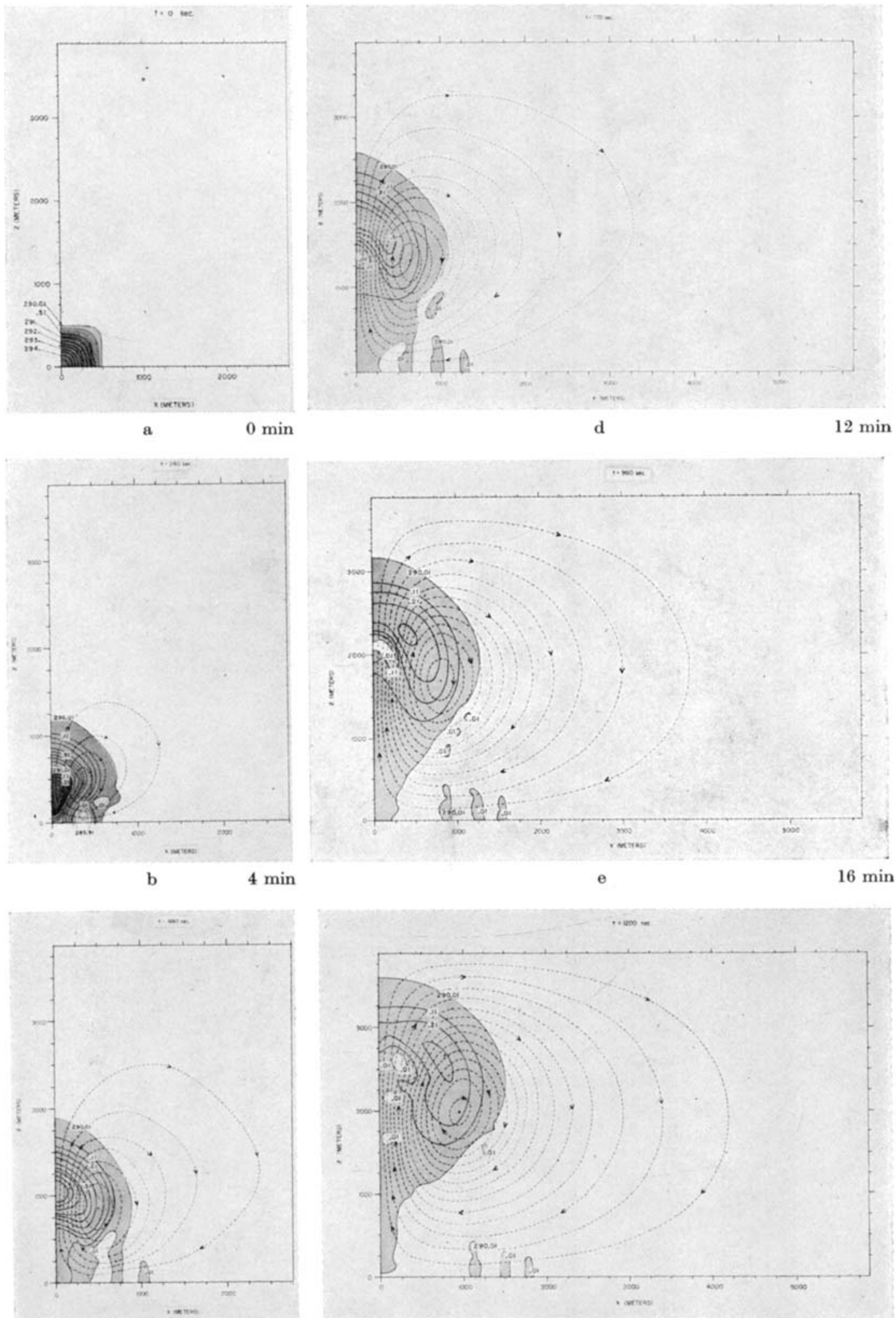

a 0 min

d 12 min

b 4 min

e 16 min

FIG. 13a–f. Experiment 100. Maps at 4-minute intervals. Stream lines are drawn at intervals of 1000 g/cm sec.

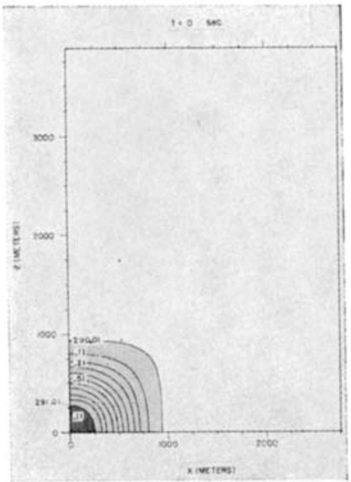

a 0 min

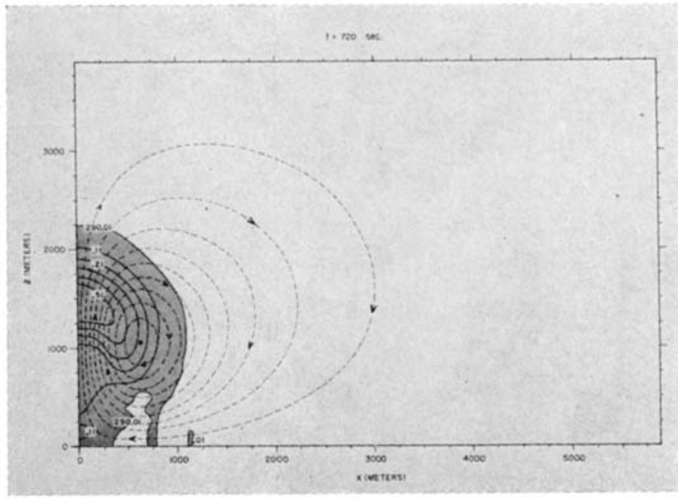

d 12 min

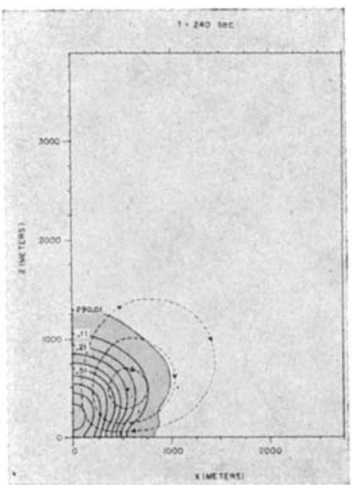

b 4 min

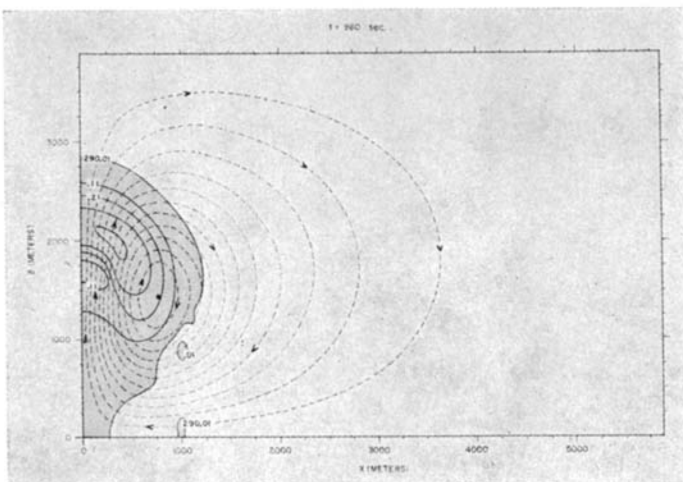

e 16 min

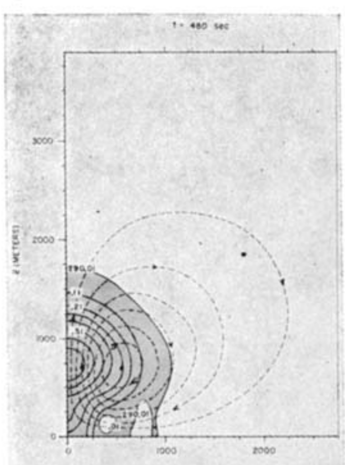

c 8 min

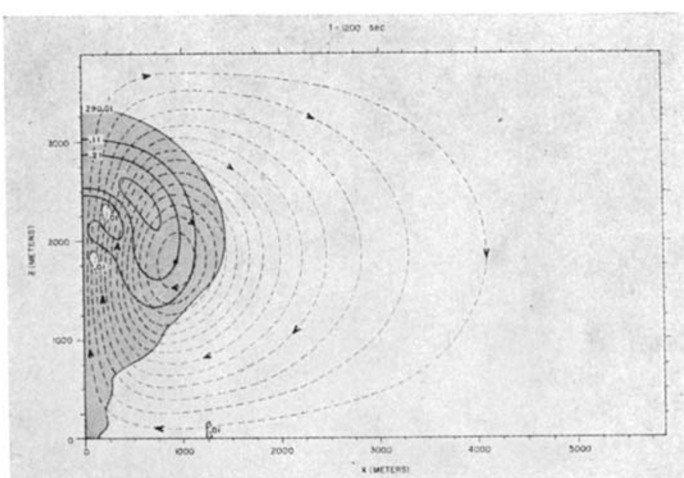

f 20 min

Fig. 14*a–f*. Experiment 101. Maps at 4-minute intervals. Stream lines are drawn at intervals of 0001 g/cm sec.

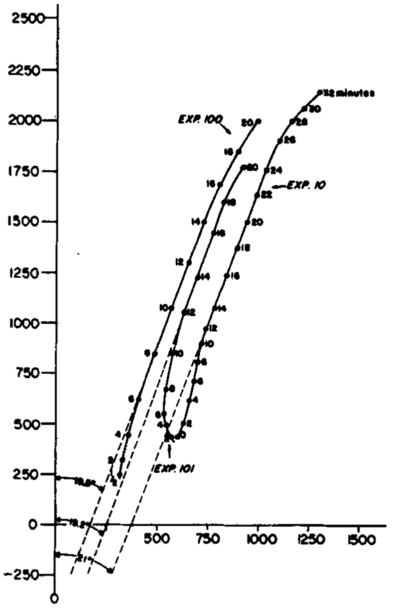

FIG. 15. Trajectories of the vortex centers for experiments 10, 100, and 101. Tangents are drawn to the straight line portions of the curves.

heights of the following significant features, of experiments nos. 10, 100, and 101: (*a*) the maximum potential temperature value; (*b*) the vortex centers; and (*c*) the maximum vertical momentum. All these heights have been visually interpolated from grid-point values and slightly smoothed. In particular the first few minutes of (*c*) for no. 10 were somewhat affected by the

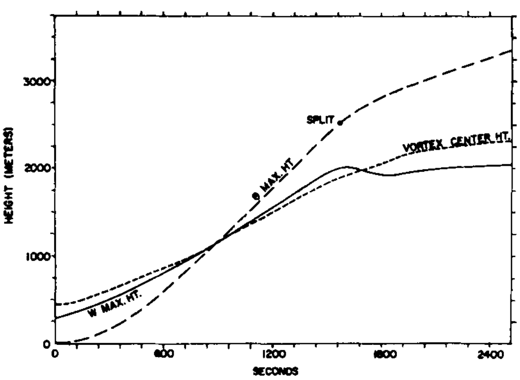

a

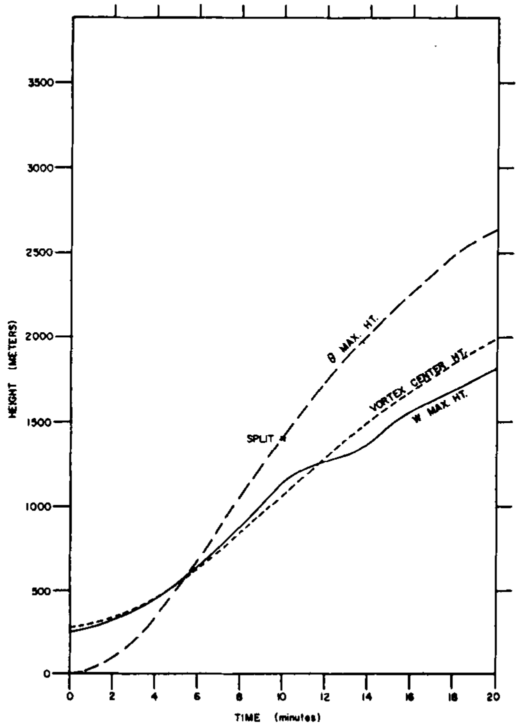

b

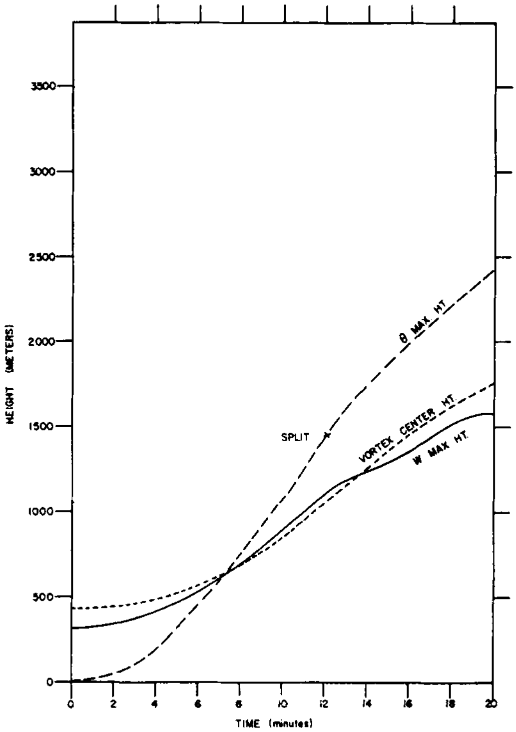

c

FIG. 16*a*, *b*, *c*. Heights of significant features of experiments 10, 100, and 101, respectively, as functions of time. The notation "split" refers to the time at which the potential temperature maximum separates horizontally.

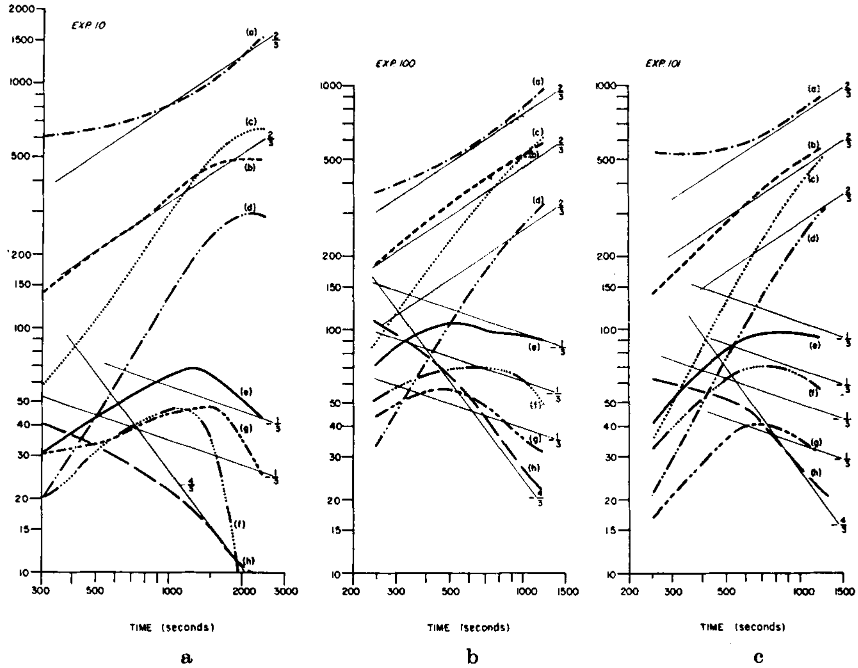

FIG. 17*a*, *b*, *c*. Values of various quantities, as functions of time, for experiments 10, 100, and 101, respectively. The scale of each quantity is arbitrary but preserved between experiments. The light solid lines are fractional powers of time.

two-point density interpolation scheme used, and part of the curve for the four-point experiment (no. 21) was used in its place. Two characteristic features of these curves may be noted and compared. About midway through the acceleration stage the three curves cross each other, after which the potential temperature maximum is higher. Later, at about the end of the acceleration stage, as the temperature maximum begins to split and form the characteristic "mushroom" shape, the vertical motion maximum falls behind and subsequently trails the vortex center. For uniformly accelerating thermals it may be shown by dimensional arguments that these events should occur in no. 100 at half the height and 1/8 of the elapsed time of the values in no. 10, and indeed this is approximately true. From figure 16*c* we see, however, that a similar ratio exists between no. 10 and no. 101, which was not theoretically predicted. Furthermore if one superimposes the curves for nos. 100 and 101, with a small change of origin, the last ten minutes are virtually identical. One cannot similarly superimpose no. 10 on either of the two. It appears, therefore, that the changes in results are due entirely to the increased resolution.

We now further investigate the approach to the similarity stage by examining the behavior of a number of quantitative properties of the experiments. Figs. 17*a*, *b*, *c*, are time curves, on a log-log scale, of the following quantities, for experiments nos. 10 and 100, and no. 101 respectively: (*a*) the distance of the vortex center from the center line; (*b*) the maximum value of the (approximate) stream function; (*c*) the total released potential energy; (*d*) the total kinetic energy; (*e*) the maximum value of vertical momentum; (*f*) the rate of change of total kinetic energy; (*g*) the energy dissipation rate; and (*h*) the maximum value of potential temperature. The ordinate scales of the curves are arbitrary but quantities (*c*)–(*d*) and (*f*)–(*g*) are on the same scale and a given quantity may be compared between experiments. Relations (23) indicate that in the similarity stage the first four quantities should be proportional to $t^{2/3}$ (slope of $\frac{2}{3}$ on the log-log scale) the next three to $t^{-1/3}$ and the last to $t^{-4/3}$. From these curves it appears that the similarity stage was not fully attained in any of the experiments, though the high resolution cases approached much closer. We also observe that the various fields do not approach this stage uniformly. In particular the kinetic energy and the closely related maximum vertical momentum continue to increase after some other quantities have nearly reached equilibrium.

It is hypothesized that this difficulty is caused by the viscosity-diffusion terms in two different ways, both related to the relative change in disturbance scale and grid separation. In the first place, if energy is transferred from low to high wave numbers by non-linear processes, it will be somewhat misleading to look at the total kinetic energy as a function of time when the disturbance scale is continually increasing, since this increase creates more and more intermediate scales for energy to pass through on its way to the grid scale and ultimate removal from the system. Without a Fourier analysis of the energy spectrum, however, it is impossible to show whether this effect is important. The apparent smoothness of the stream pattern tends to cast some doubt. Furthermore a true energy cascade is probably not possible in a two-dimensional system. This suggests that the real difficulty consists of a lack of communication between the energy containing scale of motions and the grid scale, when these are widely separated. Thus a correct numerical simulation of the kinematics may require a three-dimensional net, although a fair approximation to the mean flow pattern can perhaps be obtained by use of a turbulent length scale related to the main disturbance scale rather than the grid.

It would obviously be desirable to again double the number of grid points to test these hypotheses. For the present model, and with present computational facilities this is impractical, requiring a complete revision of the machine code and a rather large amount of computation time.

In view of the apparent approach to the similarity stage, it is of interest to compare values of certain characteristic features and parameters with those obtained from Richards' experimental results. In Table 2 columns A–E are figures obtained from Richards' analysis of 5 experimental realizations. Columns labeled nos. 100 and 101 refer to the results of these experiments at times of 14 and 15 minutes, respectively, when the curves of Fig. 17 indicated about the closest approach to similarity. The error percentage is Richards' qualitative estimate of his observational error for a given realization. It does not seem possible to make similar estimates of error for the present results because of their non-randomness and dependence on physical and mathematical assumptions. The quantities evaluated in each row are the following:

n—the ratio of Z, the "virtual height" of the thermal "front" to the thermal's radius at its widest point, R. The virtual height is the height from the virtual origin, determined in the present experiments from the vortex trajectory curves (Fig. 15). The position of the thermal front and sides were measured arbitrarily from the 0.01 degree isentrope.

c—the ratio of the virtual heights of the widest part of the thermal to that of its front.

$-\dot{E}_K/\dot{E}_P$—the ratio of the rate of increase of total kinetic energy to that of loss of available potential energy.

$C/Z\dot{Z}$—the ratio of circulation, $C = \oint \mathbf{V}\cdot d\mathbf{S}$, to the product of the height of the thermal front and its velocity, where the circulation integral was taken around one side of the thermal. The circulation would equal $\int_{-\infty}^{\infty} u_3(0, x_3)\, dx_3$ if there were no boundary effects, and actually this is the major contribution to it.

$w_{\max}/\dot{Z}$—the ratio of the maximum value of vertical velocity (also the maximum scalar velocity) to the rate of ascent of the thermal front.

$\dot{Z} \Big/ \sqrt{\frac{g}{R}\iint \Delta\varrho/\bar{\varrho}\, dx_1\, dx_3}$—a quantity proportional to the square root of the ratio of the kinetic energy of the thermal rising as a solid body to its potential energy, essentially the reciprocal of the square root of the drag coefficient.

It is evident from the first two rows that the numerical simulation yields too tall and narrow an element. The figures in the next three rows indicate that the velocities are too large relative to the thermal's ascent rate, and the last row shows that the ascent rate itself is too large. All of the above data appear to lead to a conclusion that the motions of the system are insufficiently damped. At the same time there is no evidence of any form of computational instability. Thus we may conclude that *computational dissipation sufficient to insure com-*

TABLE 2. *Physical experiment.*

Quantity	A	B	C	D	E	± Error %	Avg.	Numerical experiment No. 100	No. 101
n	2.02	2.20	2.11	2.49	1.86	5	2.14	3.0	2.96
c	0.54	0.48	0.53	0.56	0.47	8	0.52	0.67	0.64
$-\hat{E}_K/\hat{E}_P$	0.40	0.33	0.37	0.22	0.58	15	0.38	0.62	0.64
$C/Z\dot{Z}$	1.14	0.91	1.36	0.65	1.40	12	1.09	1.47	1.44
$w_{max}/\dot{Z}$	1.5	1.4	1.8	1.0	1.6	10	1.46	1.9	1.95
$\dot{Z} \Big/ \sqrt{\frac{g}{R}\iint \frac{\Delta\varrho}{\varrho}\, dx_1\, dx_3}$	0.69	0.88	0.65	0.64	0.68	8	0.71	0.72	0.71

putational stability is less than that required to simulate the observed dynamics. It is doubtful that this conclusion has been definitely established for any previous numerically integrated hydrodynamic system, nor could it be so established without the aid of a good set of laboratory measurements of the phenomenon being simulated. We believe this to be one of the most significant results of this series of experiments.

6. Summary

Our efforts to develop a numerical model capable of simulating dry convective motions have evidently been partially successful. Motions generated from reasonably physical initial conditions developed in a qualitatively correct manner and remained computationally stable. Although the equations admit types of motions of no particular interest here (sound waves) which were not completely excluded by the initial conditions, they remained completely innocuous and it was not in general necessary to account for their energetics. The truncation errors associated with the various linear and advective terms of the finite difference equations evidently had little effect upon the computational results after the initial period of linear accleration because of the smoothing imposed by the viscosity-diffusion terms and because of the scale separation of the principal energy containing motions and the grid interval. Thus computations performed with somewhat different finite difference formulations yielded essentially identical results.

The principal reason for both the success and the deficiencies of these experimental results lies in the use of Smagorinsky's method of simulation of eddy-exchange processes, which are assumed to connect the explicit and molecular scales of motion. Results of the computations indicate that the eddy exchange terms partially satisfy a real physical requirement, and that their effects in insuring computational stability, though practically important, are incidental. This is shown by the fact that a completely stable computation may have insufficient small-scale damping to simulate laboratory experimental results. The most suitable form of the eddy coefficients, thus far obtained primarily from dimensional analysis, remains somewhat indefinite, especially in regard to the turbulent length scale and the equilibrium assumption in stable regions.

In view of the moderate success thus far attained it would seem justifiable to continue along the general path outlined in the first section as follows:

(1) Continue development of time-dependent computational models, to include:

(*a*) development of a sound-filtered model, similar to the Malkus–Witt model but suitable for small-amplitude disturbances in a deep or shallow gas layer or incompressible fluid; this is desirable in view of the impracticability of simulating motions in an incompressible, or nearly incompressible, fluid with the present model and the evident insignificance of the elasticity terms for even deep gas layers, provided the buoyancy is relatively small;

(*b*) improvement of the dissipation formulation by elimination of the equilibrium assumption and possible use of a turbulent length scale determined by the flow.

(c) development of an axially symmetric model with possible inclusion of the tangential velocity component; eventual development of a truly three-dimensional model;

(d) development of models to include condensation, evaporation, and eventually precipitation effects.

(2) Further test the computational models by application to one or more of the following suitable laboratory-tested experiments:

(a) instantaneous point source convection (axially symmetric);

(b) continuous point and/or line source convection and convection in an unstable fluid without boundary disturbances.

(c) convection in stratified environments, and with basic velocity fields.

(3) Perform numerical experiments with the models simulating conditions beyond the capacity of controlled physical experiments, in particular:

(a) large amplitude convection, such as that following a bomb explosion;

(b) cloud convection, with and without precipitation and rotation effects.

In addition to this long-range program it would be of interest to pursue a little further the simulation of instantaneous line source convection. It seems that one of the basic difficulties in attaining the similarity stage is the economic problem of providing sufficient resolution so that the thermal includes a large number of grid points for a considerable period of time without running into boundaries. A possible manner of circumventing this difficulty is to apply the similarity solutions to reduce the order of the equations. If the incompressible equations (with the Boussinesq approximations) are written in non-dimensional form and the characteristic length, density deviation and time are related by expressions (23) the time variation can be eliminated from the system. The system then can probably be solved by iterative methods to yield a steady-state or quasi-steady-state solution in the non-dimensional variables. Comparison of such solutions for varying resolutions and turbulent exchange formulations should lead to a more exact understanding of the effects of these factors.

7. Acknowledgements

Thanks are gratefully tendered to Drs. J. Smagorinsky, S. Manabe, and K. Bryan, for their valuable suggestions and continuing interest in this work; to Mrs. E. Arnold, who was responsible for most of the computer programming; and to Mr. E. Rayfield and Mrs. J. Snyder, who respectively drafted the figures and typed the manuscript.

REFERENCES

BATCHELOR, G. K., 1954, Heat convection and buoyancy effects in fluid. *Quart. Jr. Roy. Meteor. Soc.*, **80**, p. 339.

—— 1956, *The Theory of Homogeneous Turbulence.* Cambridge University Press, Cambridge, 197 pp.

BLAIR, A., METROPOLIS, N., VON NEUMANN, J., TAUB, A. H., and TSINGOU, M., 1959, A study of a numerical solution to a two dimensional hydrodynamical problem. *Math. Tables and Other Aids to Computation*, **13**, p. 145.

CORRSIN, S., and KISTLER, A. L., 1955, Free stream boundaries of turbulent flows. *NACA Report No.* **1244**.

COURANT, E., ISAACSON, E., and REES, M., 1952, On the solution of non-linear hyperbolic differential equations by finite differences. *Comm. Pure and Applied Math.*, **5**, p. 243.

ELIASSEN, A., 1956, A procedure for numerical integration of the primitive equations of the two-parameter model of the atmosphere. University of California at Los Angeles, Dept. of Meteorology, *Scientific Report No.* **4**, on contract AF 19(604)-1286, 53 pp.

ELLISON, T. H., 1957, Turbulent transport of heat and momentum from an infinite rough plane. *J. Fluid Mech.*, **2**, p. 456.

ESTOQUE, M. A., 1961, A theoretical investigation of the Sea breeze. *Quart. Journ. Roy. Meteor. Soc.*, **87**, pp. 136–146.

HEISENBERG, W., 1948, Zur statistischen Theorie der Turbulenz. *Z. Physik*, **124**, p. 628.

KASAHARA, A., 1960, A numerical experiment on the development of a tropical cyclone. University of Chicago, Dept. of Meteorology, *Technical Report No.* **12** to U.S. Weather Bureau, 85 pp.

KAZANSKY, A. B., and MONIN, A. S., 1956, Turbulence in the inversion layer near the surface. *Izv. Akad. Nauk, S.S.S.R.*, Ser. Geofyz., No. **1**.

KOLMOGOROFF, A. N., 1941, The local structure of turbulence in incompressible viscous fluid for very large Reynolds numbers. *C. R. Acad. Sci., U.R.S.S.*, **30**, p. 301.

KUO, H. L., 1960, Solution of the non-linear equations of cellular convection and heat transport. M.I.T. Dept of Meteorology, *Scientific Report No.* **3**, Planetary Circulations Project, October 1960, 43 pp.

LILLY, D. K., 1961, A proposed staggered-grid system for numerical integration of dynamic equations. *Monthly Weather Review*, **89**, p. 59.

MALKUS, J. S., and WITT, G., 1959, The evolution of a convective element: a numerical calculation. *The Atmosphere and the Sea in Motion* (the Rossby Memorial Volume), Rockefeller Institute Press, New York, 509 pp.

MALKUS, W. V. R., and VERNOIS, G., 1958, Finite amplitude convection. *J. Fluid Mech.*, **4**, p. 225.

PHILLIPS, N. A., 1956, The general circulation of the atmosphere: a numerical experiment. *Quart. Journ. Roy. Meteor. Soc.*, **82**, p. 123.

—— 1959, An example of non-linear computational instability. *The Atmosphere and the Sea in Motion* (the Rossby Memorial Volume). Rockefeller Institute Press, New York, 509 pp.

—— 1960, Calculations for the hemisphere with the barotropic primitive equations. Paper presented at the International Symposium on Numerical Weather Prediction, Tokyo, Japan, November 7–13, 1960.

RICHARDS, R. S. 1959, *Int. J. Air Pollution* **1**, pp. 198–220.

RICHARDSON, L. F., 1926, Atmospheric diffusion shown on a distance-neighbor graph. *Proc. Roy. Soc.* (London), **110**, p. 709.

RICHTMYER, R. D., 1957, *Difference Methods for Initial Value Problems.* Interscience Publishers, Inc., New York, 238 pp.

SASAKI, Y., 1960, Effects of condensation evaporation and rainfall on the development of mesoscale disturbances: a numerical experiment. The A and M College of Texas, Dept of Meteorology and Oceanography, *Tech. Report No.* **5**, Project 208 Contract No. NSF-G7417.

SCHLICHTING, H., 1935, Turbulenz bei Wärmeschichtung. *Zeit. angew. Math. u. Mech.*, **15**, p. 313, Translation by J. Vanier, U.S. NACA, Tech. Memo. 1262, Oct. 1950.

SCORER, R. S., 1957, Experiments on convection of isolated masses of buoyant fluid. *J. Fluid Mech.*, **2**, p. 583.

—— 1958, *Natural Aerodynamics.* Pergamon Press, London, 312 pp.

—— 1959, The behavior of chimney plumes, *Int. Journ. of Air Pollution*, **1**, p. 198.

SCORER, R. S., and LUDLAM, F. H., 1953, Bubble theory of penetrative convection, *Quart. J. Roy. Meteor. Soc.*, **79**, p. 94.

SCORER, J. M., 1962. To be published in Int. J. Air Pollution.

SHUMAN, F. G., 1960, A numerical study of nonlinear computational instability. Paper presented at the Third Numerical Weather Prediction Conference, 27–30 June 1960, Chicago, Ill.

SMAGORINSKY, J., 1958, On the numerical integration of the primitive equations of motion for baroclinic flow in a closed region. *Monthly Weather Review*, **86**, p. 457.

SUTTON, O. G., 1953, *Micrometeorology.* McGraw-Hill, New York, 333 pp.

WOODWARD, B., 1959, The motion in and around isolated thermals. *Quart. J. Roy. Meteor. Soc.*, **85**, p. 144.